ChemBioChem

Chemistry Europe
European Chemical Societies Publishing
ChemBioChem

RESEARCH ARTICLE OPEN ACCESS

A DNA-Based Binding Assay for the m^{6}A-RNA Reader Proteins

Rajiv Kumar Bedi | Amedeo Caflisch

Department of Biochemistry, University of Zurich, Zurich, Switzerland

Correspondence: Amedeo Caflisch (caflisch@bioc.uzh.ch)

Received: 17 November 2025 | **Revised:** 4 February 2026 | **Accepted:** 5 February 2026

Keywords: 6mA-DNA | epitranscriptomics | fluorescence polarization | m^{6}A-RNA | RNA binding proteins

ABSTRACT

N6-methyladenosine (m^{6}A) is the most prevalent internal modification in eukaryotic messenger RNA. Dysregulation of m^{6}A-RNA signaling has been implicated in a wide range of human diseases. The N6-methyladenosine modifications in DNA (6mA) is much rarer, and its role is still debated. Here, we report the first holo crystal structure of the m^{6}A-RNA reader YTHDC2. The 1.6 Å resolution structure of YTHDC2 bound to the single-strand (ss) hexanucleotide GG(6mA)CTA-DNA shows an essentially identical binding mode of (6mA)CT-DNA as (m^{6}A)CU-RNA in the other four human reader proteins YTHDC1 and YTHDF1-3. Comparative analysis of the binding of fluorescent-labeled 6mA-ssDNA and m^{6}A-RNA revealed that the five human m^{6}A-RNA readers exhibit slightly stronger binding affinity for 6mA-modified DNA with a factor ranging from about 1.3 for YTHDC1 to 30 for YTHDC2. Given the similar affinity and the similar binding mode of 6mA-ssDNA and m^{6}A-RNA, we set up to develop a fluorescence polarization (FP) binding assay that uses a fluorescent-labeled 6mA-containing ssDNA as probe. The DNA-based FP assay shows high stability and robustness, making it suitable for high-throughput screening applications. The assay provides a powerful and cost-efficient platform to accelerate the discovery of small-molecule modulators targeting m^{6}A-RNA reader proteins.

1 | Introduction

Messenger RNA (mRNA) undergoes diverse chemical modifications that modulate its function and fate. Among these, N^6-methyladenosine (m^{6}A)—methylation at the nitrogen-6 position of adenosine within the consensus DRACH motif (D = A, G, or U; R = A or G; H = A, C, or U)—is the most abundant internal modification in eukaryotic mRNA [1]. m^{6}A marks are enriched in noncoding regions, particularly around stop codons and within the 3′ untranslated region (3′ UTR), and their distribution is dynamic across tissues, developmental stages, and stress conditions [2]. The m^{6}A modification influences key aspects of mRNA metabolism, including splicing, stability, translation, and nuclear export, through the coordinated action of writer-, eraser-, and reader-proteins [3]. The methyltransferase complex (METTL3–METTL14) installs m^{6}A on RNA, while FTO and ALKBH5 remove it [4–6]. Reader proteins, particularly those containing YTH domains (YTHDF1–3, YTHDC1, YTHDC2), recognize m^{6}A-modified transcripts to regulate their fate, either by promoting translation or directing degradation [7].

Abnormal m^{6}A-RNA regulation has been linked to numerous human diseases, including metabolic disorders, cardiovascular disease, fibrosis, and cancer, making m^{6}A-modifying enzymes and readers promising therapeutic targets [8]. Consequently, biochemical assays capable of quantifying interactions between small molecules and m^{6}A regulatory proteins are essential for drug discovery. Our laboratory previously established an m^{6}A reader-based homogeneous time-resolved fluorescence assay using natural m^{6}A-binding proteins, while other groups have developed fluorescence polarization (FP) assays employing m^{6}A-modified RNA probes [9, 10].

N6-methyladenine (6mA) in DNA is chemically analogous to the well-characterized m^{6}A, yet its existence and biological relevance in mammals remain controversial. Although low levels of 6mA have been reported, multiple studies have failed to detect 6mA in

mouse tissues, cultured human cells, or human placental mitochondrial DNA [11, 12]. In contrast, trace amounts have been identified in DNA from mouse, human, and glioblastoma samples, raising the possibility that 6mA may be present at extremely low levels [13]. Recent evidence further suggests that a portion of mammalian 6mA may arise indirectly, through incorporation of deoxy-6mA produced from RNA-derived m^6A via nucleotide salvage pathways, rather than through a dedicated DNA methyltransferase [14]. One proposed functional consequence of 6mA in DNA is the suppression of mutagenesis. The methylation of the adenosine amino group destabilizes mismatched 6mA:8-oxo-dG pairs and can reduce misincorporation by DNA polymerase β, thereby limiting mutagenic 8-oxo-dGTP incorporation [15]. A recent study shows that the m^6A reader YTHDF3 binds to 6mA in DNA and recruits ALKBH1 to excise 6mA from genomic DNA, offering the first functional in vivo evidence that a m^6A reader acts on DNA to remove 6mA [16].

Here, we report the first holo crystal structure of the YTH domain (i.e., m^6A-RNA reader module) of YTHDC2. The complex with 6mA-modified ssDNA provides structural insight into 6mA recognition. Inspired by this structure, we developed a ssDNA-based FP assay to evaluate the binding of (small) molecules into the recognition pocket of human YTH readers. The assay was benchmarked against its RNA counterpart and applied in competitive binding experiments to determine IC_{50} values for the canonical GG(m^6A)CU motif and selected small-molecule binders. Finally, we validated the high-throughput suitability of the DNA-based FP assay using Z-factor analysis, demonstrating its potential for screening compounds targeting m^6A-RNA reader proteins.

2 | Results and Discussion

We first present the crystallography results followed by the development of the FP assay based on the 6mA-ssDNA fluorescent probe. To simplify the notation, we use DNA instead of ssDNA in the following.

2.1 | X-Ray Crystal Structure of 6mA-DNA Bound to YTHDC2

After several unsuccessful attempts to determine the crystal structure of YTHDC2 in the complex with m^6A-RNA by co-crystallization, we decided to try with 6mA-DNA. The complex of the YTHDC2 reader domain and GG(6mA)CTA-DNA crystallized in the C2221 space group at 1.6 Å resolution, with one protein monomer present in the asymmetric unit. The overall architecture closely resembles previously reported YTH domain structures bound to m^6A-containing RNA (Figure 1) [17–20]. Structural superposition of the YTHDC2–DNA complex (PDB 9SZP) with the complex of YTHDC1 and GG(m^6A)CU-RNA (PDB 4R3I) results in a backbone (C-alpha) RMSD of 0.87 Å for 130 of the 136 backbone atoms of YTHDC2, indicating a highly conserved core fold and the same recognition mode of methylated (desoxy-)adenosine. As in canonical RNA-bound YTH domains, the 6mA base is accommodated within a hydrophobic aromatic cage formed by W1310, W1360, and L1365 (Figure 1A,C). The adenine ring also forms the characteristic hydrogen-bonding interactions previously observed in m^6A–RNA complexes, underscoring that the fundamental mechanism of m^6A discrimination is preserved in the DNA-bound state.

The 6mA and the adjacent 3′ C-T/U nucleotides overlay closely between the DNA- and RNA-bound structures, suggesting that recognition of this core sequence is structurally robust to the sugar–phosphate context. Additionally, the guanidinium group of R1401 in YTHDC2 is positioned between G2 and C4, forming stabilizing cation–π interactions that further reinforce the DNA conformation (Figure 1B,C). In contrast, the two 5′ guanosines adopt distinct conformations. In the DNA-bound YTHDC2 complex, G1 and G2 are stabilized through crystal packing interactions with nucleotides of a neighboring asymmetric unit, whereas in the YTHDC1–RNA complex these residues are solvent exposed and more flexible. The 5′ terminal A6 is partly stabilized by stacking with T5, while its opposing face remains solvent-exposed. The comparison of the 6mA-DNA-bound YTHDC2 structure with the corresponding YTHDC1 crystal structure (PDB: 6WE9) reveals a similar binding pattern (Figure S1), in which the 6mA base and the 3′ nucleotides closely superimpose, whereas the 5′ nucleotides diverge due to differences in oligonucleotide length used for co-crystallization, leading to distinct crystal packing interactions.

2.2 | Titration of the Reader Proteins to the Fluorescent Labeled 6mA-DNA and m^6A-RNA

Inspired by the identical binding mode of 6mA-DNA and m^6A-RNA, we aimed to develop an FP assay for m^6A reader proteins that uses a 6mA-DNA probe. Because FP measurements rely on the difference in molecular weight between the free fluorophore and the fluorophore–protein complex, we cloned the YTH domains of the five human m^6A reader proteins with an N-terminal GST tag to increase the molecular weight and thereby enhance the polarization signal. Each GST-tagged YTH domain was expressed and purified in assay buffer, and binding affinities were determined by titrating the purified proteins against 3 nM fluorescein-labeled DNA or RNA probe. The resulting EC_{50} values are summarized in Figure 2A (DNA) and Figure 2B (RNA).

The three cytoplasmic YTHDF proteins (YTHDF1, YTHDF2, and YTHDF3) exhibited comparable binding affinities toward the RNA probe, with EC_{50} values ranging from 20 to 60 nM, consistent with their high sequence and structural similarity reported previously [21]. In contrast, the nuclear YTHDC proteins showed more divergent affinities: YTHDC1 bound the RNA probe with high affinity ($EC_{50} \approx 5$ nM), whereas YTHDC2 displayed substantially weaker binding ($EC_{50} \approx 297$ nM).

Notably, all five reader proteins exhibited stronger binding to the DNA probe than to the corresponding RNA probe, with YTHDC2 showing the most pronounced difference—approximately a 30-fold ratio. The increased binding strength observed with DNA may be attributed to the lack of the 2′-hydroxyl group, which allows shorter hydrogen bond distances and minimizes steric hindrance relative to RNA, as previously reported [22]. While their study reports slightly stronger binding of YTHDF1 and YTHDF2 to mRNA than to DNA (factor of about 2 and 1.5, respectively), the observed differences may arise from variations in the primary sequence and length of the oligonucleotides used.

To evaluate signal stability, the same assay plates were maintained at room temperature and remeasured over a 24-h period. The maximum raw polarization (mFP) values are shown in Figure 2C (DNA) and Figure 2D (RNA). The DNA probe signal

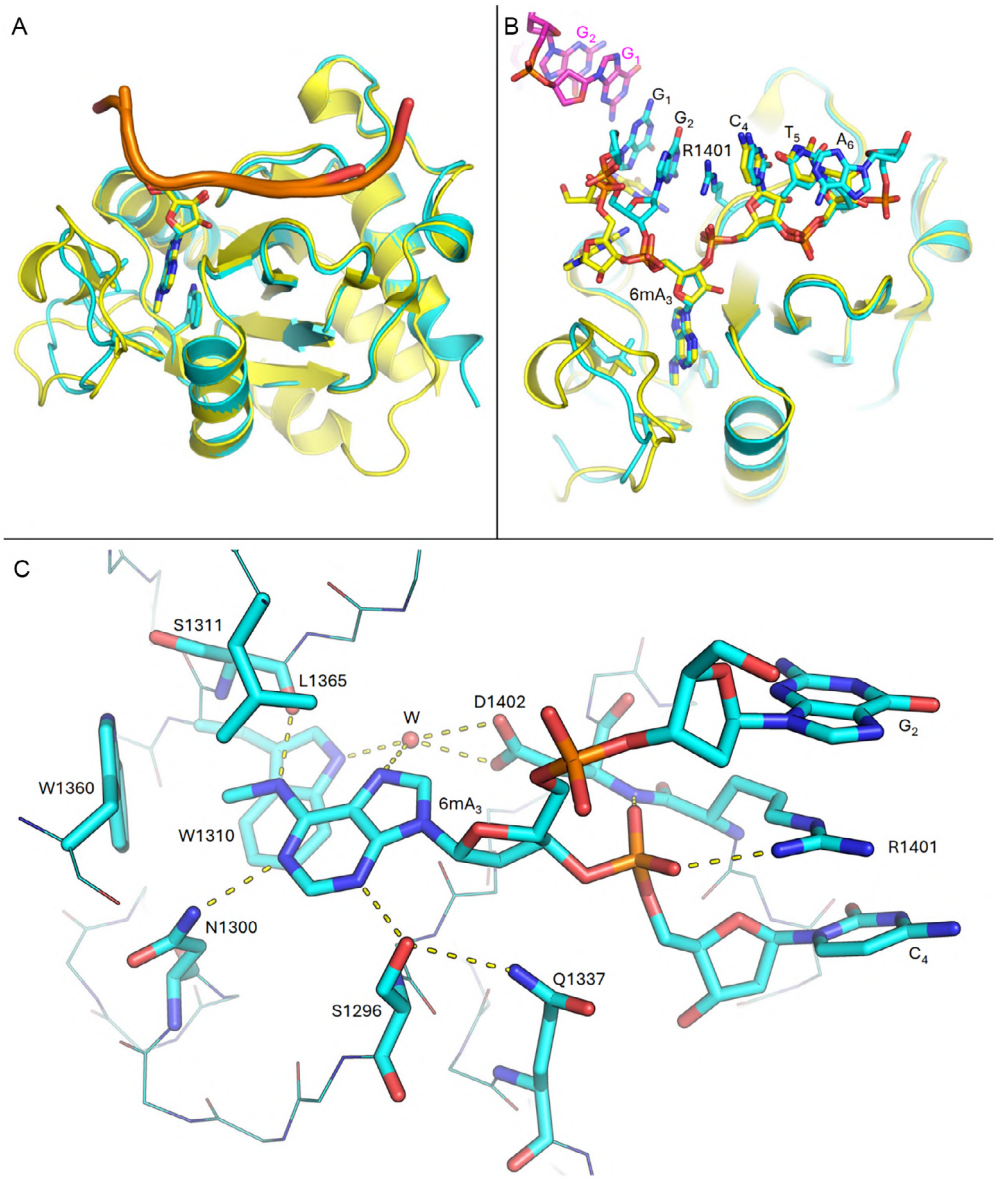

FIGURE 1 | Comparison of 6mA-DNA-bound YTHDC2 (cyan, PDB code: 9SZP) with m^{6}A-RNA bound YTHDC1 (yellow, PDB code: 4R3I). (A) Ribbon representation of the oligoDNA/RNA with the aromatic cage-forming residues. (B) Details of the oligoDNA (carbon atoms in cyan) and oligoRNA (carbon atoms in yellow). The two DNA bases G1 and G2 from a neighboring 6mA-DNA/YTHDC2 complex are also shown (magenta). (C) Zoom-in on the key interactions of 6mA DNA with the YTHDC2 binding pocket residues (sticks, YTHDC2 numbering) along with the conserved water molecule (red sphere).

remained stable throughout the 24-h interval, whereas the RNA probe signal gradually decreased, likely due to RNA degradation or autocatalytic cleavage under assay conditions.

2.3 | Competition FP Assay

The crystal structure of the 6mA-DNA/YTHDC2 complex showed the same binding mode as for m^{6}A-RNA (Figure 1). Moreover, the raw signal in the titration assay was more stable over time for 6mA-DNA than m^{6}A-RNA (Figure 2C,D). Thus, we decided to establish an FP competition assay that makes use of fluorescein-labeled 6mA-DNA (DNA tracer). Following the titration assays, the dose–response data were fitted, and each reader protein was subsequently used in the competition experiments at a concentration corresponding to its EC_{60} value. Competition assays were performed for measuring the binding of (i) unlabeled GG(m^{6}A)CU-RNA against all five reader proteins (Figure 3) and (ii) with selected small-molecule compounds against YTHDC1, YTHDC2, and YTHDF2 (Figure 4).

In both (DNA-FP and RNA-FP) assay formats, GG(m^{6}A)CU-RNA efficiently displaced the fluorescein-labeled probes from YTHDC1, consistent with the high affinity of YTHDC1 observed in the titration experiments. For the DNA probe assay, GG(m^{6}A)CU-RNA also displaced the bound probe from YTHDF1, YTHDF2, and YTHDF3 with similar IC_{50} values of 14–45 μM. In the RNA probe assays, displacement was observed for YTHDF2 and YTHDF3 ($IC_{50} \approx 15$ and 32 μM, respectively), whereas YTHDF1 showed only partial displacement, reaching approximately 50% inhibition at the highest concentrations tested. In contrast, GG(m^{6}A)CU-RNA did not displace either the DNA- or RNA-bound probe from YTHDC2, in agreement with

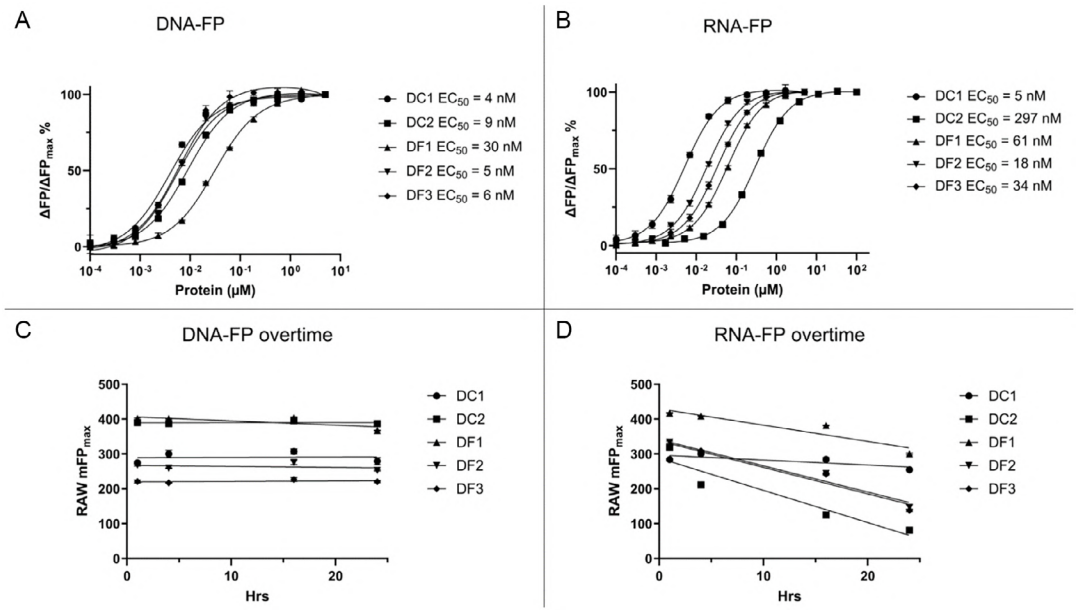

FIGURE 2 | Comparison of the binding of fluorescent-labeled 17-mer 6mA-DNA and m^{6}A-RNA to the five human m^{6}A-RNA reader proteins. (A, B) Titration curves of the reader proteins to the 6mA-DNA (A) and m^{6}A-RNA (B). (C,D) Time dependence of the maximum raw FP signal of 6mA-DNA (C) and m^{6}A-RNA (D). The concentration of the fluorescein-labeled DNA or RNA probe was 3 nM. In the legends here and in the following figures, the reader proteins are abbreviated, e.g., DC1 for YTHDC1. The data points are displayed as the average of four replicates. Error bars here and in Figures 3 and 4 are standard deviations. Most standard deviations are not visible because they are smaller than the size of the symbols used for the data points.

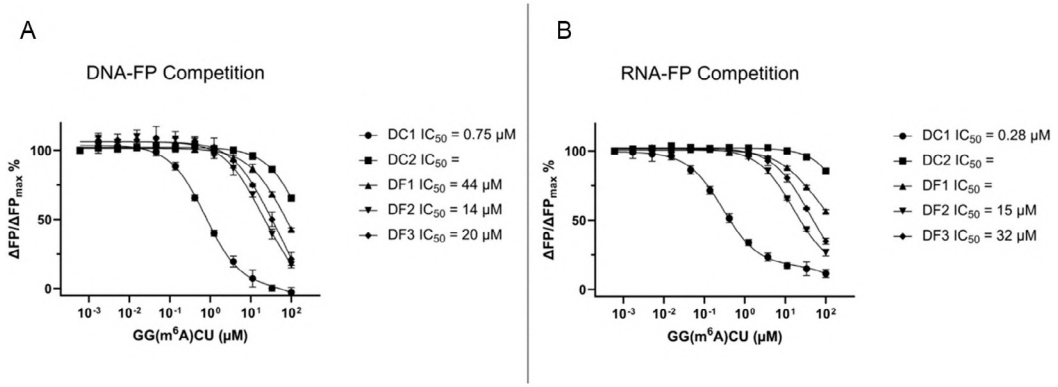

FIGURE 3 | Competitive displacement of 17-mer fluorescent-labeled 6mA-DNA probe (A) and m^{6}A-RNA probe (B) by unlabeled pentameric GG(m^{6}A)CU-RNA. The concentration of the fluorescent probe was 3 nM. The concentration of the reader protein was determined from the EC$_{60}$ values obtained from the protein titration (Figure 2). For the DNA–FP competition assay, the concentrations were 7, 13, 48, 9, and 9 nM for DC1, DC2, DF1, DF2, and DF3, respectively. For the RNA–FP competition assay, the concentrations were 8, 410, 86, 26, and 48 nM for DC1, DC2, DF1, DF2, and DF3, respectively.

the weak RNA-binding affinity of YTHDC2 measured in the initial titration experiments. All five m^{6}A readers exhibited strong binding to the DNA or RNA probe in the titration assay, with affinities in the low nanomolar range (Figure 2A,B), whereas micromolar affinities were observed in the competition assay (Figure 3). This difference likely arises from the longer length of the DNA (17-mer; 5′-FAM-AAGAACCGG(6mA)CTAAGCT-3′) or RNA (5′-FAM-AAGAACCGG(m^{6}A)CUAAGCU-3′) probe, which allows for additional favorable electrostatic interactions (salt bridges between the phosphate groups and the basic side chains on the recognition surface of the reader proteins), compared with the shorter pentameric RNA (5′-GG(m^{6}A)CU-3′) used in the competition assay.

For the DNA-based FP competition assay, we selected YTHDC1, YTHDC2, and YTHDF2 as representative reader proteins. Three small-molecule compounds were tested (Figure 4). Compound **1** (i.e., compound **23** of Ref. [23]) is selective for YTHDF2, while compounds **2** and **3** (compounds **17** and **30** of Ref. [23], respectively) show activity across the YTH family [23]. Compound **1** displayed strong selectivity toward YTHDF2, with an IC$_{50}$ of 1.9 μM while showing substantially weaker binding to YTHDC1 and YTHDC2 (IC$_{50}$ values of 188 and 752 μM, respectively). In contrast, compounds **2** and **3** inhibited all three reader proteins with low micromolar IC$_{50}$ values.

2.4 | High Quality of the DNA-Based FP Assay for High-Throughput Screening (Z-Factor Test)

Assay performance was evaluated using positive and negative controls across a 384-well plate format (Figure 5). The FP values for

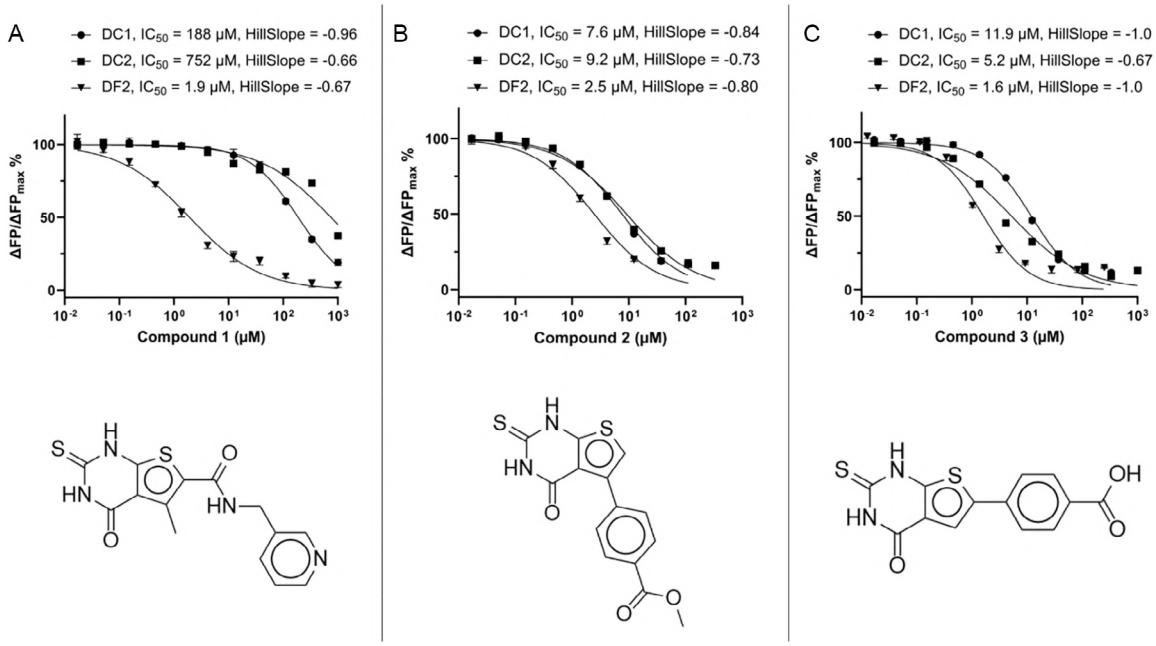

FIGURE 4 | Dose-response curves derived from the competitive DNA-FP assay for the three reader proteins along with the 2D structures of the YTHDF2 ligands **1–3**. The concentration of DC1, DC2, and DF2 was 7, 13, and 9 nM, respectively, and the concentration of the fluorescent labeled 6mA-DNA was 3 nM.

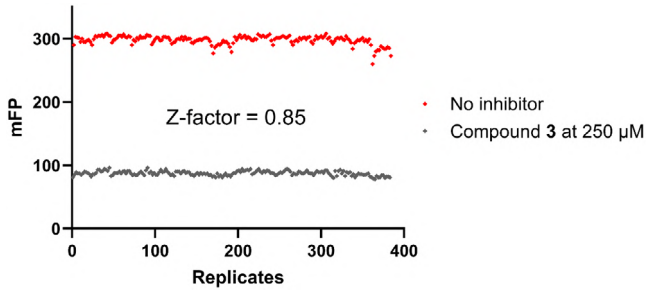

FIGURE 5 | High-throughput compatibility test. The test was carried out in a 384-well plate using YTHDC2 at a concentration of 13 nM and fluorescent-labeled 6mA-DNA at 3 nM, with alternating well containing the inhibitor **3** at 250 μM.

the positive control averaged 297 mFP (SD = 7), while the negative control averaged 87 mFP (SD = 3.6). The separation band is large resulting in a Z-factor of 0.85, which indicates excellent assay robustness and reproducibility [24]. Signal-to-background (Mean signal ÷ Mean background) and signal-to-noise ratios ([Mean signal – Mean background] ÷ SD background) were 3.4 and 58.3, respectively, further confirming the suitability of the assay for high-throughput screening applications.

3 | Conclusions

We have reported the first crystal structure of the YTHDC2 reader domain bound to a nucleic acid. The binding mode of 6mA-DNA in YTHDC2 is essentially identical to the canonical binding mode of m^{6}A-RNA by the other human reader proteins. The YTHDC2/6mA-DNA structure and the slightly higher affinity of the reader domains for 6mA-DNA than m^{6}A-RNA motivated us to develop a FP binding assay based on fluorescent-labeled 6mA-DNA. A robust FP assay based on competition with a DNA tracer was established for the five human m^{6}A-RNA reader proteins, and it was validated first by measuring the binding of GG(m^{6}A)CU-RNA. Notably, the assay performance is high as measured in a 384-well plate format (Z-factor of 0.85), and thus, it can be used for high-throughput screening. Compared with the RNA-based FP assay, the DNA-based assay is more robust and cost-effective, as modified DNA oligos are more stable and less expensive than modified RNA oligos. In addition, the use of DNA eliminates the need for an RNase-free setup. The DNA-based FP assay will play a substantial role in hit identification and the development of chemical probes for the human m^{6}A-RNA reader proteins.

4 | Experimental Section

4.1 | Crystallization, Data Collection, and Structure Solution

The DNA sequence encoding the YTH domain of human YTHDC2 (residues 1285–1424) with an N-terminal His6 tag was cloned into the pETDuet-1 vector using the BamHI and XhoI restriction sites. The recombinant construct was transformed into *E. coli* Rosetta (DE3) cells, and protein expression was induced with 200 μM isopropyl β-D-1-thiogalactopyranoside (IPTG) at 20°C for 16 h. Cells were harvested by centrifugation and resuspended in lysis buffer containing 100 mM Tris–HCl (pH 8.0) and 500 mM NaCl. Cell lysis was performed by sonication, and the lysate was clarified by centrifugation at 20,000 rpm for 1 h at 4°C. The supernatant was loaded onto a 5 mL HisTrap FF Ni-NTA affinity column (GE Healthcare). After washing with buffer containing 100 mM Tris–HCl (pH 8.0), 500 mM NaCl, and 50 mM imidazole, the bound protein was eluted with buffer containing 100 mM Tris–HCl (pH 8.0), 500 mM NaCl, and 250 mM

imidazole. The N-terminal His6 tag was removed by cleavage with tobacco etch virus (TEV) protease overnight at 4°C. Imidazole was removed by dialysis, and the sample was subjected to a secondary subtractive Ni-NTA chromatography step to remove TEV protease and uncleaved protein. The final purification was carried out by size-exclusion chromatography using a Superdex 75 16/600 column (GE Healthcare) equilibrated with 10 mM Tris–HCl (pH 7.4) and 150 mM NaCl.

The purified YTHDC2 YTH domain was concentrated to 10 mg/mL and mixed with 1 mM single-stranded DNA containing the GG(6mA)CTA sequence (synthesized by Microsynth AG). The protein–DNA mixture was incubated for 1 h at 4°C prior to setting up crystallization trials using commercial screening kits. Crystals of the complex were obtained in a solution containing 20% (w/v) PEG 3350 and 200 mM KNO_3. Diffraction data were collected at beamline P13 of the Deutsches Elektronen-Synchrotron (DESY), Hamburg. The data were processed using autoPROC [25]. The structure was solved by molecular replacement with Phaser (as implemented in the Phenix package), using the YTHDC1 YTH domain structure (PDB ID: 4R3I) as the search model. Model building and refinement were performed using COOT and phenix.refine, respectively [26, 27]. Data collection and refinement statistics are presented in Table 1.

TABLE 1 | Data collection and refinement statistics table.

Data collection	
Wavelength (Å)	1.05965
Resolution range (Å)	34.2–1.578 (1.65–1.58)
Space group	C 2 2 21
Unit cell (a b c (Å), α, β, γ (°))	74.57 115.469 39.951, 90 90 90
Total reflections	288,134 (2094)
Unique reflections	53,390 (1016)
Multiplicity	5.4 (2.1)
Completeness (%)	97.97 (85.67)
Mean I/sigma (I)	5.21 (0.06)
Wilson B-factor	18.15
R-merge	0.127 (6.916)
R-meas	0.1394 (8.98)
R-pim	0.0566 (5.635)
$CC_{1/2}$	0.995
Refinement	
Reflections used in refinement	23,718 (2564)
Reflections used for R-free	1146 (118)
R-work	0.1993 (0.3169)
R-free	0.2310 (0.3436)
RMS bonds (Å)	0.006
RMS angles (°)	0.82
Ramachandran favored (%)	97.76
Ramachandran allowed (%)	2.24
Ramachandran outliers (%)	0
Rotamer outliers (%)	0
Clashscore	2.08
Average B-factor	22.51
Average macromolecules B-factor	20.08
Average solvent B-factor	31.43

Statistics for the highest resolution shell is shown in parentheses.

4.2 | Protein Expression and Purification for Fluorescence Polarization

The DNA sequences encoding the human YTH domains ($YTHDC1_{345–509}$, $YTHDC2_{1285–1424}$, $YTHDF1_{361–559}$, $YTHDF2_{383–579}$, and $YTHDF3_{391–585}$) were amplified and cloned into the pGEX-6P-1 vector using the BamHI and XhoI restriction sites to generate N-terminal GST-tagged constructs. The template plasmids were a gift from Cheryl Arrowsmith, Elisa Izaurralde, Markus Landthaler, and Chuan He (Addgene plasmids #64652, #148487, #64653, #38089, and #70088). Recombinant proteins were overexpressed in *E. coli* Rosetta (DE3) cells induced with 200 μM isopropyl β-D-1-thiogalactopyranoside (IPTG) at 20°C for 16 h. Cells were harvested by centrifugation and resuspended in lysis buffer containing 100 mM Tris–HCl (pH 8.0) and 500 mM NaCl. Cell lysis was performed by sonication, and the lysate was clarified by centrifugation at 20,000 rpm for 1 h at 4°C. The supernatant was loaded onto a glutathione Sepharose 4B column (GE Healthcare), and bound proteins were eluted with buffer containing 10 mM reduced glutathione, 100 mM Tris–HCl (pH 8.0), and 500 mM NaCl. The GST-tagged proteins were further purified by size-exclusion chromatography using a HiLoad 16/600 Superdex 200 pg column (GE Healthcare) equilibrated in 10 mM Tris–HCl (pH 8.0) and 150 mM NaCl. SDS-PAGE showing the protein purity and the 260/280 ratios is presented in Figure S2.

4.3 | Titration Assay

A 17-mer single-stranded DNA probe containing an N6-methyladenosine modification (5′-FAM-AAGAACCGG(6mA)CTAAGCT-3′) was purchased from Microsynth AG. The corresponding RNA probe (5′-FAM-AAGAACCGG(m^6A)CUAAGCU-3′) was kindly provided by Bioduro-Sundia (China). The probe concentration was maintained at 3 nM in all assays. Measurements were performed in black 384-well plates (Corning, Cat. No. 3575) in a total reaction volume of 50 μL, and each data point represents the average of four replicates. The assay buffer contained 20 mM Tris–HCl (pH 7.4), 150 mM NaCl, and 0.01% (w/v) BSA.

For FP titrations, serial threefold dilutions of each reader protein were prepared, ranging from 100 to 0.0001 μM, in the presence of 3 nM probe. The mixtures were incubated for 1 h at 25°C before measurement. Polarization values were recorded using a Tecan SPARK plate reader equipped with 485/20 nm excitation and 535/25 nm emission polarization filters suitable for fluorescein detection. Binding curves were generated by fitting the data to a nonlinear dose–response model in GraphPad Prism, from which EC_{50} values were derived. To monitor signal stability, the same plate was remeasured at multiple time points over a 24 h period, and the mFP values were compared.

4.4 | Competition Assay

For the FP–based competition assays, the protein concentration corresponding to the EC_{60} value for each reader protein (YTHDC1, YTHDC2, YTHDF1, YTHDF2, and YTHDF3) was selected based on the titration curves. To assess competition with nucleic acid ligands, the GG(m^6A)CU-RNA pentamer was serially diluted threefold from 100 to 0.0006 μM and incubated with the protein–probe complex under the same buffer conditions described above.

For compound competition assays, selected small-molecule inhibitors were serially diluted threefold from 1000 to 0.04 μM. The value of FP was measured after 1 h of incubation at 25°C using the same settings as described for the titration assays.

4.5 | Z-Factor Test

To determine assay robustness, solutions containing YTHDC2 along with the 6mA-DNA probe in assay buffer were dispensed into alternating wells across the plate, while the intervening wells contained equivalent volumes of solution with YTHDC2 inhibitor.

The Z-factor was calculated according to the equation: $1 - \frac{3(\sigma_p + \sigma_n)}{|\mu_p - \mu_n|}$

where σ_p and σ_n are the standard deviations, and μ_p and μ_n are the mean FP values of the positive (no inhibitor) and negative (with inhibitor) wells, respectively [24].

Acknowledgments

The authors thank Dr. Görkem Kurtuldu for her help with setting up protein crystallization trials. The synchrotron data was collected at P13 beamline operated by EMBL Hamburg at the PETRA III storage ring (DESY, Hamburg, Germany). We would like to thank Michael Agthe for the assistance in using the beamline and Francesco Nai for helpful discussions. We thank Annalisa Invernizzi for providing compounds **1**-**3**. We thank the Lotte und Adolf Hotz-Sprenger Stiftung for financial support.

Open access publishing facilitated by Universitat Zurich, as part of the Wiley - Universitat Zurich agreement via the Consortium Of Swiss Academic Libraries.

Funding

This work was supported by Lotte und Adolf Hotz-Sprenger Stiftung.

Data Availability Statement

The atomic coordinates and structure factors for the X-ray crystal structure reported in this study have been deposited in the Protein Data Bank under accession code 9SZP.

References

1. D. Dominissini, S. Moshitch-Moshkovitz, S. Schwartz, et al., "Topology of the Human and Mouse m6A RNA Methylomes Revealed by m6A-Seq," *Nature* 485 (2012): 201–206.

2. K. D. Meyer, Y. Saletore, P. Zumbo, O. Elemento, C. E. Mason, and S. R. Jaffrey, "Comprehensive Analysis of mRNA Methylation Reveals Enrichment in 3′ UTRs and near Stop Codons," *Cell* 149 (2012): 1635–1646, https://doi.org/10.1016/j.cell.2012.05.003.

3. S. Zaccara, R. J. Ries, and S. R. Jaffrey, "Reading, Writing and Erasing mRNA Methylation," *Nature Reviews Molecular Cell Biology* 20 (2019): 608–624.

4. J. Liu, Y. Yue, D. Han, et al., "A METTL3–METTL14 Complex Mediates Mammalian Nuclear RNA N6-Adenosine Methylation," *Nature Chemical Biology* 10 (2014): 93–95.

5. G. Jia, Y. Fu, X. Zhao, et al., "N6-Methyladenosine in Nuclear RNA Is a Major Substrate of the Obesity-Associated FTO," *Nature Chemical Biology* 7 (2011): 885–887.

6. G. Zheng, J. A. Dahl, Y. Niu, et al., "ALKBH5 Is a Mammalian RNA Demethylase that Impacts RNA Metabolism and Mouse Fertility," *Molecular Cell* 49 (2013): 18–29.

7. X. Wang, Z. Lu, A. Gomez, et al., "N6-Methyladenosine-Dependent Regulation of Messenger RNA Stability," *Nature* 505 (2014): 117–120.

8. P. C. He and C. He, "M 6 A RNA Methylation: From Mechanisms to Therapeutic Potential," *The EMBO Journal* 40 (2021): e105977, https://doi.org/10.15252/embj.2020105977.

9. C.-H. Wang and H. Zhou, "Discovery of a New Inhibitor for YTH Domain-Containing m 6 A RNA Readers," *RSC Chemical Biology* 5 (2024): 914–923.

10. L. Wiedmer, S. A. Eberle, R. K. Bedi, P. Śledź, and A. Caflisch, "A Reader-Based Assay for m6A Writers and Erasers," *Analytical Chemistry* 91 (2019): 3078–3084, https://doi.org/10.1021/acs.analchem.8b05500.

11. K. Douvlataniotis, M. Bensberg, A. Lentini, B. Gylemo, and C. E. Nestor, "No Evidence for DNA N6-Methyladenine in Mammals," *Science Advances* 6 (2020): eaay3335, https://doi.org/10.1126/sciadv.aay3335.

12. S. Schiffers, C. Ebert, R. Rahimoff, et al., "Quantitative LC–MS Provides No Evidence for m 6 dA or m 4 dC in the Genome of Mouse Embryonic Stem Cells and Tissues," *Angewandte Chemie International Edition* 56 (2017): 11268–11271.

13. Q. Xie, T. P. Wu, R. C. Gimple, et al., "N-Methyladenine DNA Modification in Glioblastoma," *Cell* 175 (2018): 1228–1243.e20.

14. M. U. Musheev, A. Baumgärtner, L. Krebs, and C. Niehrs, "The Origin of Genomic N6-Methyl-Deoxyadenosine in Mammalian Cells," *Nature Chemical Biology* 16 (2020): 630–634.

15. X. Zhang, R. M. Blumenthal, and X. Cheng, "A Role for N6-Methyladenine in DNA Damage Repair," *Trends in Biochemical Sciences* 46 (2021): 175–183.

16. X.-H. Chen, Z.-L. Wang, J. Yang, et al., "YTHDF3 Recognizes DNA N6-Methyladenine and Recruits ALKBH1 for 6mA Removal From Genomic DNA," *The EMBO Journal* 44 (2025): 4899–4917.

17. Y. Li, R. K. Bedi, E. V. Moroz-Omori, and A. Caflisch, "Structural and Dynamic Insights into Redundant Function of YTHDF Proteins," *Journal of Chemical Information and Modeling* 60 (2020): 5932–5935.

18. F. Nai, R. Nachawati, F. Zálešák, X. Wang, Y. Li, and A. Caflisch, "Fragment Ligands of the m 6 A-RNA Reader YTHDF2," *ACS Medicinal Chemistry Letters* 13 (2022): 1500–1509.

19. C. Xu, K. Liu, H. Ahmed, P. Loppnau, M. Schapira, and J. Min, "Structural Basis for the Discriminative Recognition of N6-Methyladenosine RNA by the Human YT521-B Homology Domain Family of Proteins," *Journal of Biological Chemistry* 290 (2015): 24902–24913.

20. C. Xu, X. Wang, K. Liu, et al., "Structural Basis for Selective Binding of m6A RNA by the YTHDC1 YTH Domain," *Nature Chemical Biology* 10 (2014): 927–929.

21. S. Zaccara and S. R. Jaffrey, "A Unified Model for the Function of YTHDF Proteins in Regulating m6A-Modified mRNA," *Cell* 181 (2020): 1582–1595.e18.

22. C. B. Woodcock, J. R. Horton, J. Zhou, et al., "Biochemical and Structural Basis for YTH Domain of Human YTHDC1 Binding to Methylated Adenine in DNA," *Nucleic Acids Research* 48 (2020): 10329–10341.

23. A. Invernizzi, F. Nai, R. K. Bedi, et al., "Discovery of YTHDF2 Ligands by Fragment-Based Design," *ACS Bio & Med Chem Au* 5 (2025): 753–765.

24. J.-H. Zhang, T. D. Y. Chung, and K. R. Oldenburg, "A Simple Statistical Parameter for Use in Evaluation and Validation of High Throughput Screening Assays," *SLAS Discovery* 4 (1999): 67–73.

25. C. Vonrhein, C. Flensburg, P. Keller, et al., "Data Processing and Analysis with the *autoPROC* Toolbox," *Acta Crystallographica Section D Biological Crystallography* 67 (2011): 293–302.

26. D. Liebschner, P. V. Afonine, M. L. Baker, et al., "Macromolecular Structure Determination Using X-Rays, Neutrons and Electrons: Recent Developments in Phenix," *Acta Crystallographica Section D Structural Biology* 75 (2019): 861–877, https://doi.org/10.1107/S2059798319011471.

27. P. Emsley, B. Lohkamp, W. G. Scott, and K. Cowtan, "Features and Development of Coot," *Acta Crystallographica Section D Biological Crystallography* 66 (2010): 486–506, https://doi.org/10.1107/S0907444910007493.

Supporting Information

Additional supporting information can be found online in the Supporting Information section. **Supporting Fig. S1**: Comparison of 6mA-DNA bound YTHDC2 (cyan, PDB code: 9SZP) with 6mA-DNA bound YTHDC1 (orange, PDB code: 6WE9). DNA nucleotides and the aromatic cage forming residues shown as sticks. **Supporting Fig. S2**: SDS-PAGE showing the purified GST-tagged m6A reader proteins along with their 260/280 ratios.